A new framework for optimization of variable stiffness plates

Barazanchy, Darun; van Tooren, Michel; Tatting, BF; Elham, Ali

DOI
10.2514/6.2017-0894

Publication date
2017

Document Version
Final published version

Published in
58th AIAA/ASCE/AHS/ASC Structures, Structural Dynamics, and Materials Conference

AIAA SciTech Forum
9 - 13 January 2017, Grapevine, Texas
58th AIAA/ASCE/AHS/ASC Structures, Structural Dynamics, and Materials Conference

10.2514/6.2017-0894

A new framework for optimization of variable stiffness plates

Darun Barazanchy*, Michel van Tooren† and Brian F. Tatting‡
University of South Carolina, Columbia, SC, USA
Ali Elham§
Delft University of Technology, Delft, The Netherlands

An alternative to the lamination parameters framework for optimization of variable stiffness plates is proposed that utilizes the fiber angles as design variables: the manufacturing finite element mesh (MFEM) framework. The structure and implementation of the MFEM framework allows for both stiffness and strength constraints. In this manuscript the maximum failure index is minimized for the case of static analysis, while for buckling analysis the first buckling mode is maximized. For each case examples are presented and discussed. To complete the manuscript a post-processing tool used to obtain feasible automated fiber placement machine tow paths is briefly discussed.

I. Introduction

In the last decades composites have slowly replaced metallic material in aircraft structures, however, with the introduction of the Boeing B787 and the Airbus A350 XWB composites make up more than 50% of the aircrafts weight. The increase in use of composites in primary aircraft structures has increased the use of automated fiber placement (AFP) techniques. Subsequently, designers have realized that AFP techniques allow for non-conventional layups such as fiber steered layups (variable stiffness laminates). Variable stiffness laminates allow the fiber direction to vary from point to point within a layer instead of having a constant fiber direction for the whole layer; this opens the possibility to have tailored designed laminates. These tailored designed laminates can be optimized based on the loading conditions for maximum stiffness, maximum strength, manufacturability, or any other objective functions. Variable stiffness laminates have shown unprecedented specific strength levels as reported by.[1–9]

In much of current literature[2–7,10–14] the fiber direction of variable stiffness laminates are determined using the lamination parameters. The lamination parameters allow for a continuous laminate stiffness formulation within a conservative convex solution space and limits the number of design variables when the laminate thickness is increased. This, in combination with efficient gradient based optimizers can determine the optimal the stiffness distribution to maximize structural performance in an efficient manner. A major limitation of the lamination parameters framework is the difficulty of implementing strength constraints in the optimization procedure. In addition, the lamination parameter framework is an indirect method to find the optimal fiber direction distribution since multiple stacking sequences and fiber directions can result in the same ABD-matrix. Therefore, a post-processing step is required to obtain the optimal stacking sequence.

*Ph.D. student, USC/McNAIR Center for Aerospace Innovation and Research, dbara@email.sc.edu, Member
†Professor, USC/McNAIR Center for Aerospace Innovation and Research, vantooren@cec.sc.edu, Senior Member
‡Research Assistant Professor, USC/McNAIR Center for Aerospace Innovation and Research, tatting@cec.sc.edu
§Postdoc Researcher, Flight Performance and Propulsion, a.elham@tudelft.nl, Member

The structure of this manuscript continues as follows: (ii) the fiber steering design problem and the MFEM approach are elaborated; (iii) the design variable, objective function and constraint functions are defined; (iv) multiple cases are evaluated using the MFEM framework; and finally (v) the research is summarized and future work is discussed.

II. Fiber steering design problem statement

In fiber steering the objective is to determine the optimal fiber direction ϕ^j in each point $P(x, y, z)$ in each ply j of a composite structure (a laminated plate with or without cut-outs, or a biaxial specimen etc...). The problem is defined to have a domain Ω defined in an x-y reference plane, bounded by edges Γ, loaded at the boundary by in-plane force resultants N_{nn} and N_{ns}, transverse force resultants Q_n and moment results M_{nn} and M_{ns}. A schematically representation is given in Fig. 1 to illustrate the domain Ω, the loads acting on the boundaries Γ, the deformations u, v, w, θ_x and θ_y, the distributed force perpendicular $q(x, y)$ to the plate, and the fiber direction ϕ^j in point P in ply j.

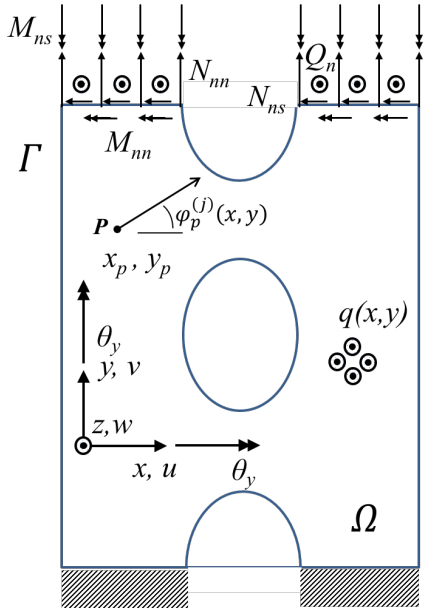

Figure 1: Schematic representation of the plate problem for fiber steering

The problem described above is implemented using a a dual mesh finite element method (FEM) approach. The first mesh (*stress-mesh*) is used to evaluate the displacements, stresses and strains within the domain. The stress-mesh is a fine mesh (to obtain converged results) with quadratic triangular elements defined by 3- or 6-nodes depending on the type of analysis, static or buckling analysis respectively. The 3-node elements have 5 degree of freedom at each node, while the 6-node elements have only 2 degree of freedom at each node. The theory behind the stress-mesh is the standard FEM approach that is well documented in the literature[15] and reported by the authors[16–19] in previous work. Besides the stress-mesh the MFEM framework utilizes a second mesh in the optimization routine,the *manufacturing-mesh* (see Fig. 2 for a schematic representation).

The dual mesh approach allows the solution to keep the number of design variables to a minimum by using a fine stress-mesh for the FEM calculations independent of the manufacturing-mesh that is used to obtain the optimized fiber direction. The manufacturing-mesh is a coarse mesh consisting of linear quadrilateral elements (4-nodes) with only 1 degree of freedom per node per ply, the fiber direction in ply k at node j.

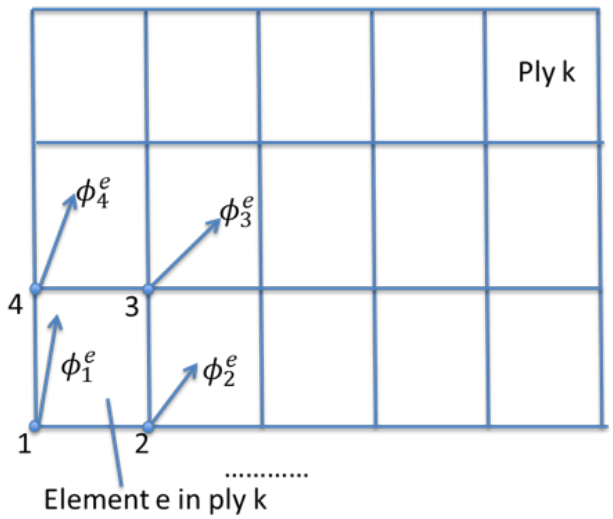

Figure 2: Manufacturing mesh representation. Each element e has four degrees of freedom in each ply k: the nodal values of the fiber direction

The fiber directions at each node are used to obtain the fiber direction distribution function using a set of four Lagrange interpolation functions

$$\begin{aligned} N_1 &= \frac{1}{4ab}(x - x_2)(y - y_4) \\ N_2 &= \frac{1}{4ab}(x - x_1)(y - y_3) \\ N_3 &= \frac{1}{4ab}(x - x_4)(y - y_2) \\ N_4 &= \frac{1}{4ab}(x - x_3)(y - y_1) \end{aligned} \tag{1}$$

where

$$a = (x_2 - x_1)/2 \qquad b = (y_4 - y_1)/2 \tag{2}$$

Therefore, the fiber direction at a point (x, y) is given as

$$\phi^{e,k} = \sum_{j=1}^{4} N_j^{(e)} \phi_j^{(e,k)} \tag{3}$$

in which the $\phi_j^{(e,k)}$ are the values of the nodal fiber direction in element e and ply k, i.e. the design variables. The two meshes are superimposed and the stress-mesh elements are mapped onto the manufacturing-mesh elements. By doing so the fiber direction can be optimized at the nodes of each manufacturing-mesh element, then the fiber directions are mapped on the centroid of the stress-mesh elements after which the displacements, stresses and strains are calculated and the constraints are evaluated.

III. Objective function and constraint functions

Material strength objective and constraint functions are implemented using the maximum failure index in the plate. In this manuscript the Tsai-Hill failure criterion (see Eq. 4) is used to quantify the failure index

in the centroid of each stress-mesh element.

$$FI = \frac{\sigma_x^2}{X^2} + \frac{\sigma_y^2}{Y^2} - \frac{\sigma_x \sigma_y}{XY} + \frac{\tau_{xy}^2}{S^2} \tag{4}$$

In addition, a manufacturing constraint function (based on the minimal allowable curvature of the slit tape) is implemented to obtain manufacturable fiber paths. The curvature is chosen in this investigation since it is the first derivative ($\frac{\mathrm{d}\phi}{\mathrm{d}s}$) of the fiber direction along the tow path.

$$\kappa = \frac{\mathrm{d}\phi}{\mathrm{d}s} = \frac{\partial \phi}{\partial x}\frac{\mathrm{d}x}{\mathrm{d}s} + \frac{\partial \phi}{\partial y}\frac{\mathrm{d}y}{\mathrm{d}s} \tag{5}$$

where

$$\mathrm{d}x = \mathrm{d}s cos(\phi) \qquad\qquad \mathrm{d}y = \mathrm{d}s sin(\phi) \tag{6}$$

Hence, the manufacturing constraint function becomes

$$\kappa(x,y) = \frac{\mathrm{d}\phi}{\mathrm{d}s} = \frac{\partial \phi}{\partial x} cos(\phi) + \frac{\partial \phi}{\partial y} sin(\phi) \tag{7}$$

where

$$\frac{\mathrm{d}\phi}{\mathrm{d}x} = \sum_{j=1}^{4} \frac{\partial N}{\partial x}\phi_j \qquad\qquad \frac{\mathrm{d}\phi}{\mathrm{d}y} = \sum_{j=1}^{4} \frac{\partial N}{\partial y}\phi_j \tag{8}$$

Furthermore, when a buckling constraint is required, the geometrical stiffness matrices are calculated to solve the eigenvalue problem

$$\big[K - \mu_j G\big] a^j = 0 \tag{9}$$

In which $\mathbf{a}^j$ is the selected buckling mode and μ_j the associated eigenvalue. The associated buckling load is found by multiplying the in-plane loads used to calculate $\mathbf{G}$ with the eigenvalue.

IV. Implementation and results

To obtain the global minimum for the MFEM framework a global search algorithm based on the basin of attraction was implemented. For a smooth objective function $f(x)$ the direction in which $f(x)$ decreases the quickest is given by the vector $-\nabla f(x)$, hence the equation of steepest descent is given by

$$\frac{d}{dt}x(t) = -\nabla f(x(t)) \tag{10}$$

The basin of attraction for steepest descent is the set of initial values resulting in the same local minimum, while generally initial values close to each other result in the steepest descent. The basin of attraction principle is illustrated in Fig. 3.[20]

To evaluate the robustness and correctness of the MFEM framework results multiple test cases are investigated. The first test case (A) consists of two design plies under a pure tensile force. To evaluate the robustness of the framework the start angles of the design plies were set to: (i) [0/0]; (ii) [90/0]; (iii) [90/90]; and (iv) [45/45]. For the second test case (B) a pure shear loading condition was investigated in which the start angles for the design plies varied were (i) [0/0] and (ii) [90/90]. Based on common composite knowledge the first test case should provide optimized plies orientated in the 0° direction, while for the second test case a ±45° orientation is expected as a result. In the two aforementioned cases the optimization is performed to obtain the minimum failure index in the plate. Additionally, a buckling problem was investigated (C)

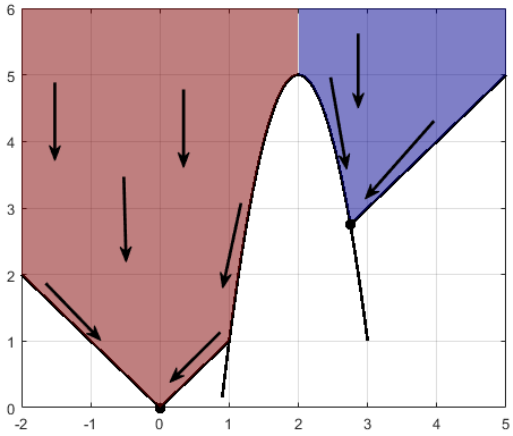

Figure 3: Two basins of attraction with the final points

in which the objective was to maximum the first buckling mode. For the buckling case the optimization is expected to produce an optimal $'S'$-shape pattern.

The plate geometries were 1000mm by 1000mm, the FEM mesh consisted of 112 triangular elements while the manufacturing mesh elements was set to 4 to limit the computational time for each optimization run. Fig. 4 shows the manufacturing mesh elements (black) on top of the finite element mesh elements (blue).

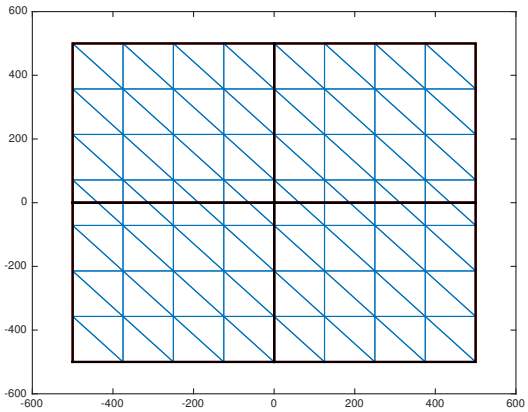

Figure 4: Manufacturing mesh elements (black) on top of the finite element mesh elements

Last, a test case (D) in which the optimal result is not intuitive (as in the previous cases) is investigated: a plate with a hole (with a radius of 150mm) under pure tension.

A. Pure tensile loading

The pure tensile boundary conditions were obtained by restricting the displacements in u on the entire left edge while only restricting the v displacement on the center node. The tensile load was applied on the nodes

on the right side edge. Both the boundary conditions and the tensile load are illustrated in Fig. 5.

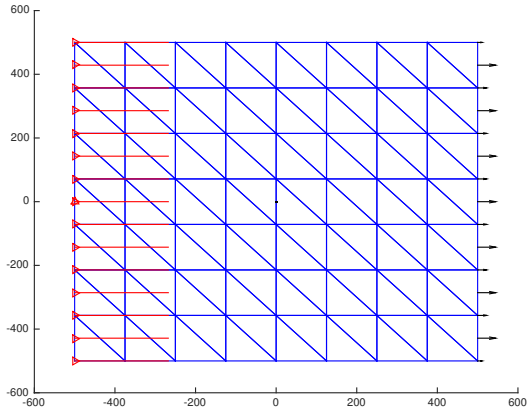

Figure 5: The boundary conditions and nodal forces in the case of pure tension

In Fig. 6 the results[a] obtained for the ±45° case using the MFEM framework are given. It can be seen from Fig. 6 that both plies were rotated to the expected and optimal orientation in case of a tensile load, 0°. Similar results were obtained for the other cases ((i) [0/0]; (ii) [90/0]; and (iii) [90/90]) and are summarized in terms of the number of function evaluations and number of successful starting points in Table 1. The MFEM framework proved it robustness by obtaining the same optimal results regardless of the chosen starting orientation angles in the design plies. The computational time and the number of function evaluations, however, did vary depending on the starting orientation angles. As it can be seen from Table. 1 the highest number of function evaluations was when the starting orientation angles was set to 0 for both plies, something which is counterintuitive. It was expected when the starting orientation angles where set to the optimal result the optimization would take less function evaluation to complete. A possible explanation for this lies in the basin of attraction method, which required a set of initial values resulting in the same local minimum. Because each chosen initial values resulted in the same results as the starting orientation angles the algorithm tested more trail points to ensure the obtained results found a global minimum, which subsequently resulted in more function evaluations.

Table 1: Pure tensile load case results

Test case	Number of function evaluations	Successful trail points
[0/0]	47620	22/22
[90/0]	21420	18/20
[90/90]	30763	10/11
[±45]	46857	11/25

[a]In this manuscript only the before and after figures for the ±45° case are shown for conciseness.

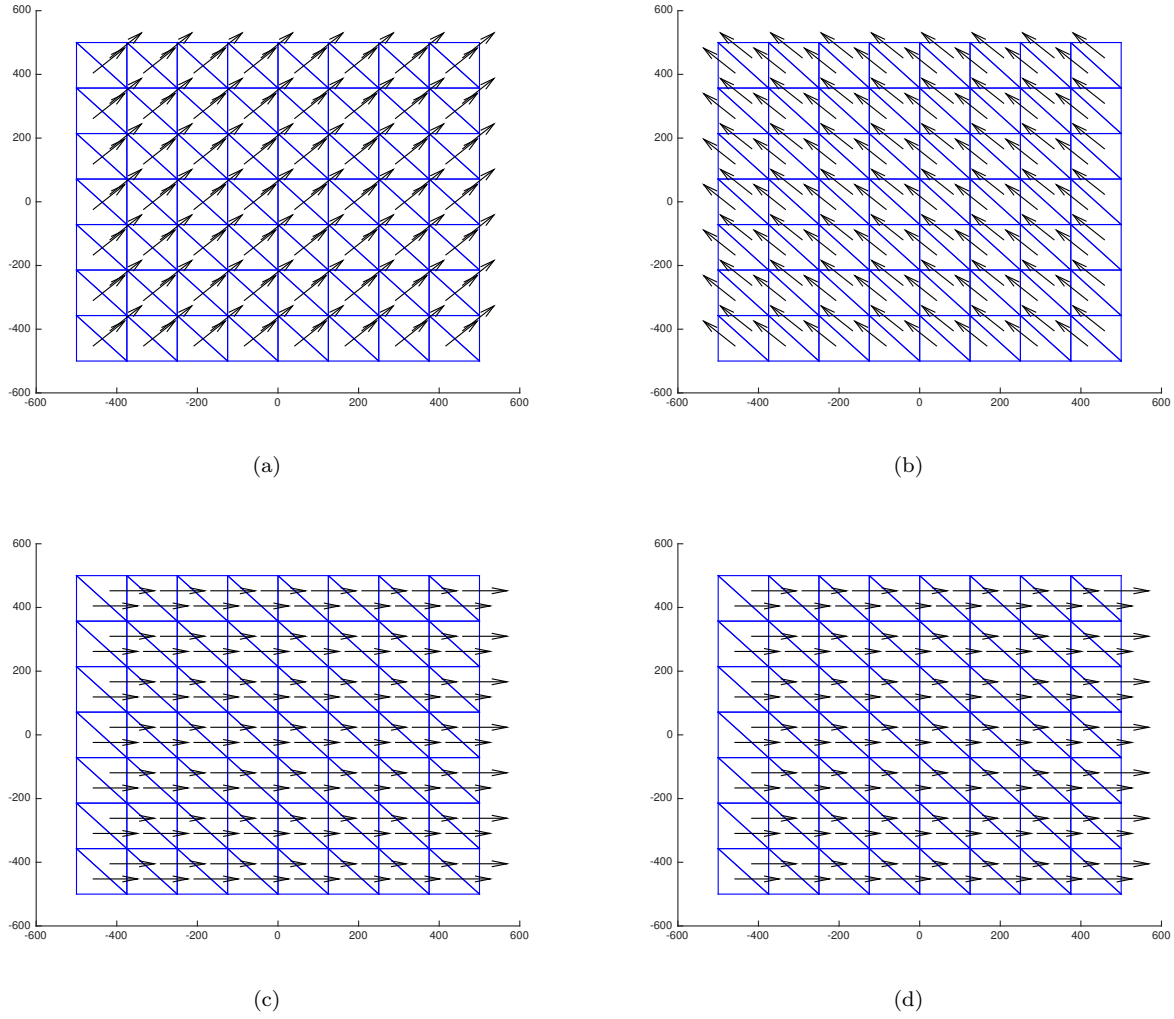

Figure 6: Fiber directions in the case of pure tension for ply 1 and 2: (a,b) before optimization; and (c,d) after optimization

B. Pure shear loading

The second test case consisted of a plate under pure shear (Fig. 7), the expected optimal results in this case are that the plies are steering toward a $\pm 45^{\circ}$ configuration. As starting orientations angles for the design plies two subcases were defined: (i) [0/0] and (ii) [90/90]. The MFEM framework managed to steer the starting orientations angles towards the expected optimal orientation, as can be seen in Fig. 8 where the before and after fiber orientations for the [0/0]-subcase are presented. The required number of function evaluations in this case was 298085 corresponding to 46 trail point of which 17 resulted in successful optimization.

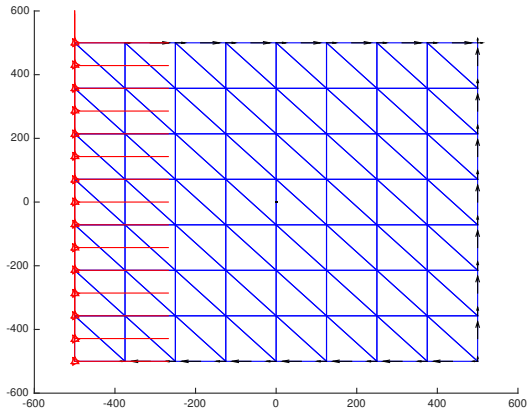

Figure 7: The boundary conditions and nodal forces in the case of pure shear

Table. 2 (which summarizes the results for both pure shear subcases) shows the effect of the starting orientation angles. When the starting orientation angles were set to 90° the optimization required less function evaluation, but more trail points to obtain the global minimum. Nevertheless, the same optimal result was obtained regardless of the starting orientation angles.

Table 2: Pure shear load case results

Test case	Number of function evaluations	Successful trail points
[0/0]	298085	17/46
[90/90]	125581	42/57

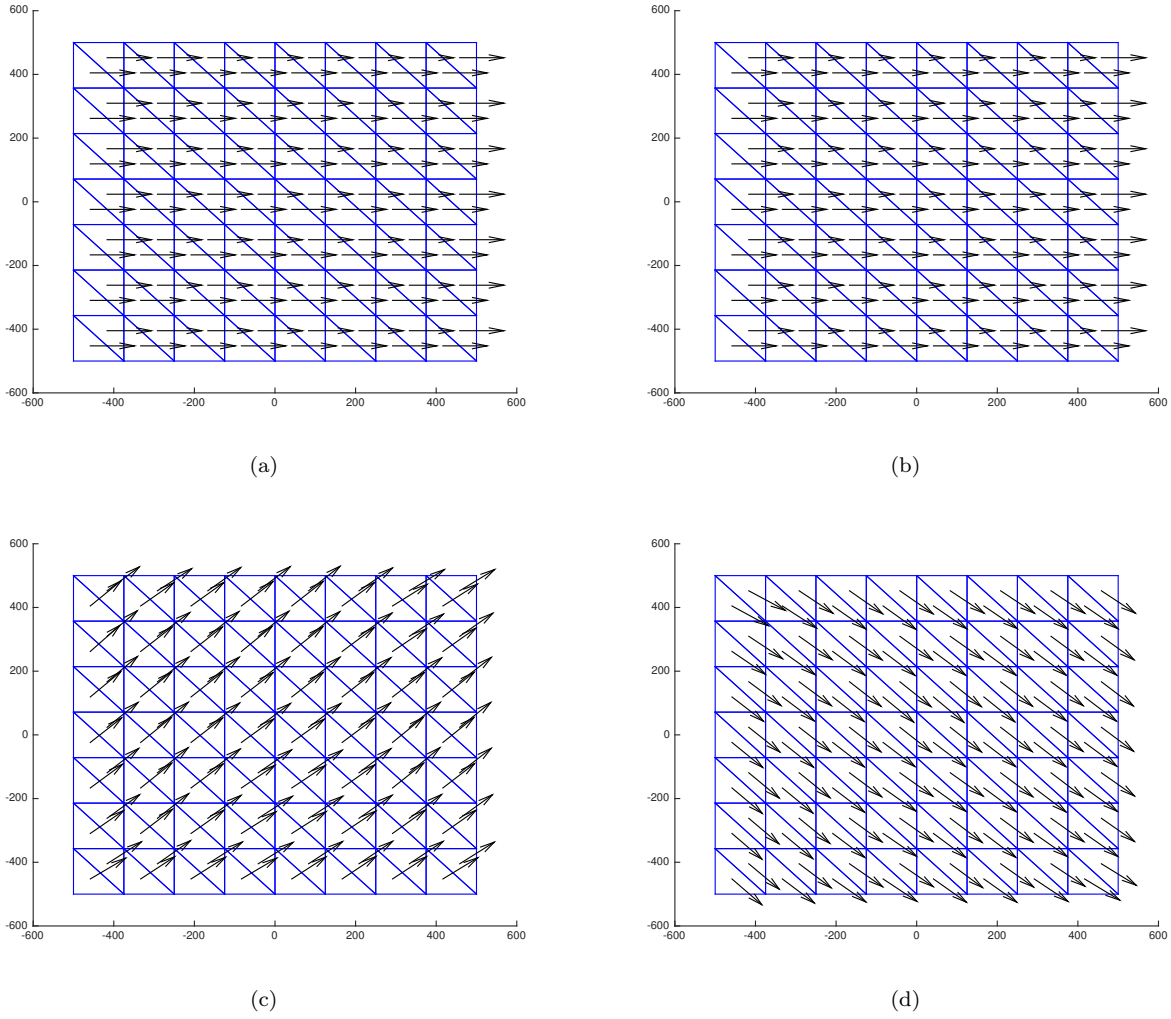

(a) (b)

(c) (d)

Figure 8: Fiber directions in the case of pure shear for ply 1 and 2: (a,b) before optimization; and (c,d) after optimization

C. Compressive loading, buckling

The third test case, a plate under a compressive load[b] (as shown in Fig. 9) was investigated. the boundary conditions in this was are shown in Fig. 9: the left edge is clamped (fixed u and v displacement), the right edge is restricted in movement in v-direction and has the nodal forces applied to it. The number of plies was reduced to 1 and its starting orientation angle was 0°. The optimal result is expected to fiber steer into an S-shape, in which the fiber on the edges are steered towards the load direction.

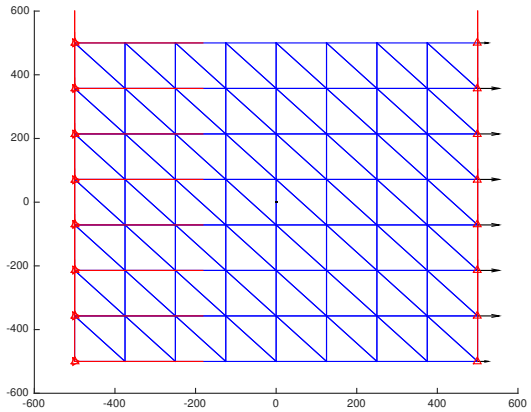

Figure 9: The boundary conditions and nodal forces in the case of buckling

The buckling analysis results are given in Fig. 10a and as expected the MFEM framework steered the fiber orientations into an S-shape. Increasing the number of manufacturing mesh elements does have an effect on the results, however, in this case (due to its simplicity) that effect is limited as can be seen from Fig. 10b and 10c. In the investigated case, buckling of a square plate under uni-axial compression it is expected buckling to occur in the middle of the plate. To maximize the buckling load the force distribution as seen by the plate is preferably shifted from a uniform distribution to an S-shape distribution (with the minimum load in the middle and the maximum on the edges). As a result the fiber near the top and bottom edge are steered towards the load direction to take up the forces. Tatting and Gürdal[9] reported similar results.

[b]It is important to note that the nodal force arrows are pointing in a positive x-direction, this is due to the plotting routine only. In the analysis the load is compressive.

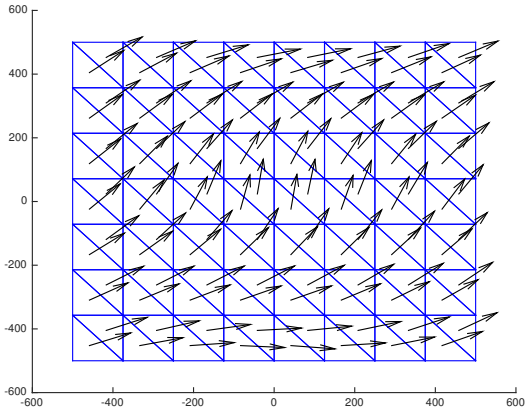

(a)

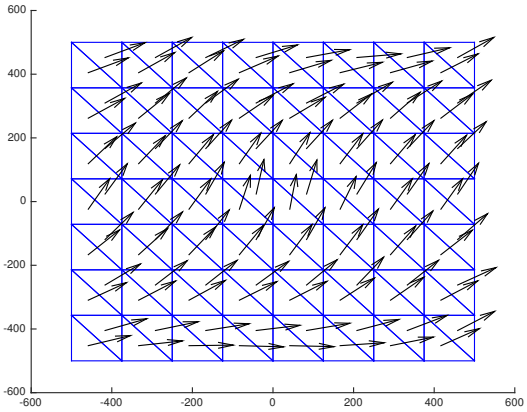

(b)

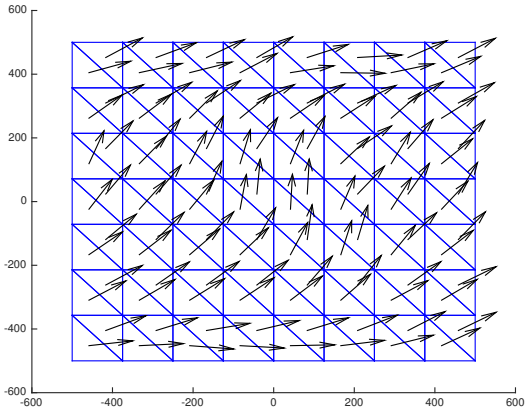

(c)

Figure 10: Fiber directions in the case of buckling: (a) using 4 manufacturing mesh elements; (b) using 16 manufacturing mesh elements; and (c) (b) using 16 manufacturing mesh elements

D. Plate with hole under pure tension

Last, a plate with a hole of a radius of 150mm under a pure tensile load was investigated. The boundary conditions and the two meshes used in the framework are shown in Fig. 11, it is important to note that due to the complexity of the problem more refined meshes were used. In this case it is difficult to determine what the optimal result will be due to the complexity of the problem, even though it seems simplistic.

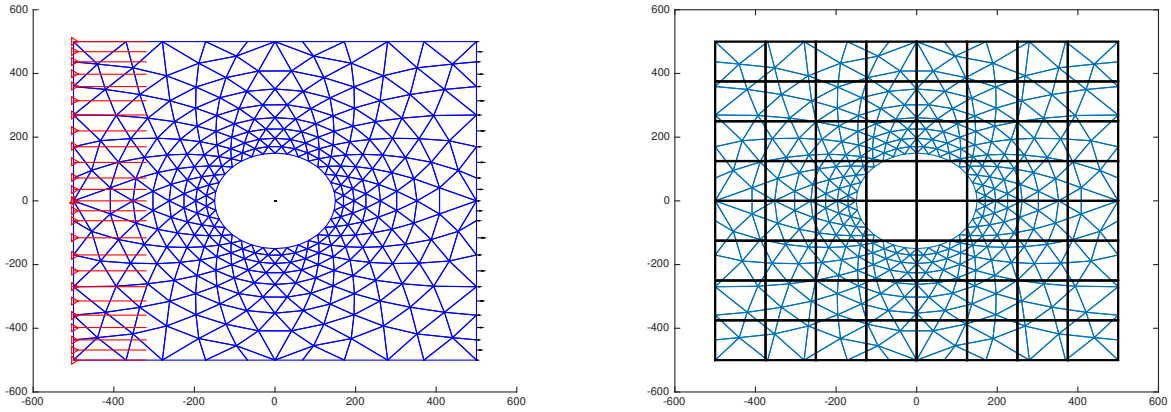

(a) (b)

Figure 11: Plate with a hole: (a) the boundary conditions; and (b) stress-mesh (blue) and manufacturing-mesh (black)

The laminate consisted of six plies in total, three design plies and three symmetry plies (for each $+\theta$ ply there was a $-\theta$ ply). The starting orientation of all three design plies was set to 0°. The fiber directions before and after the optimization are shown in Fig. 12. It is important to note that the fiber direction before optimization were the same for each ply, therefore, the figure shown is valid for all the plies. In addition, only the results for the first three plies are shown because plies 4, 5 and 6 are mirror plies of ply 3, 2 and 1, respectively.

As can be seen from Fig. 12, the fiber directions differ from the starting 0° fiber direction. The fiber directions in ply 1 and ply 2 (Fig. 12b and Fig. 12c) look similar and shows the optimizer trying to guide loads away from the hole. The fiber directions in ply 3, however, differ significantly from those in ply 1 and ply 2. To understand what is happening for ply 3 the failure index (the objective function) was investigated (see Fig. 13).

As it can be seen from Fig. 13 the maximum failure index for ply 1 and ply 2 remain the same, however, the pattern differs slightly. For ply 3 however, there is a reduction of 20% in maximum failure index and the pattern changes significantly. From these results it was concluded that the optimizer performed the requested task: minimize the maximum failure index. In addition, the results indicated the problem was more complex than initially thought. To investigate it more in depth the stresses in ply 3 before and after the optimization are examined, see Fig. 14.

From Fig. 14 it can be seen that the optimizer alleviates σ_x around the hole by placing the fiber such that σ_y and τ_{xy} are increased. Nevertheless, the maximum failure index was reduced due to the interactions between the stresses within the failure criterion.

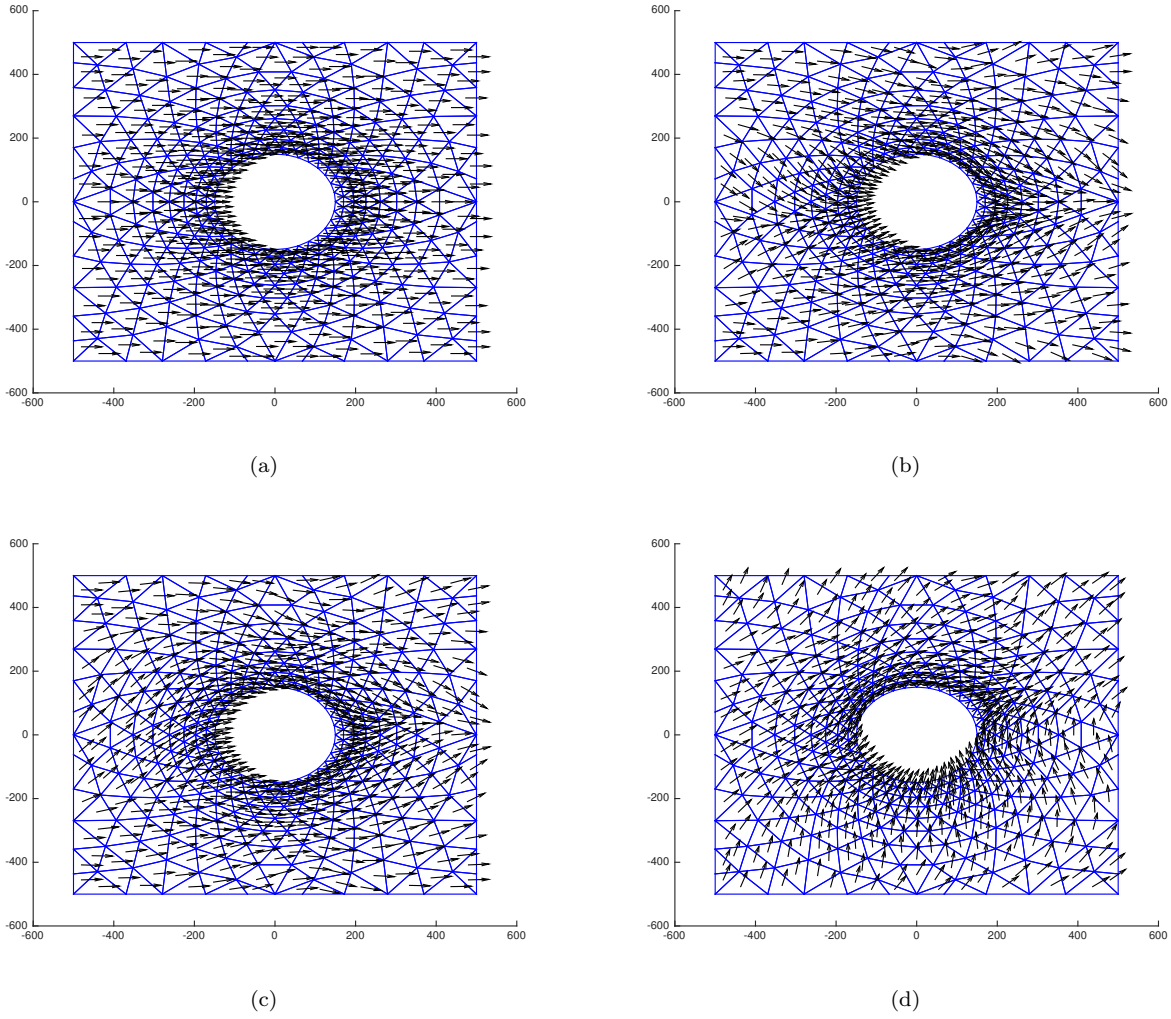

(a) (b)

(c) (d)

Figure 12: Fiber directions for a plate with a hole: (a) before optimization; and after optimization: (b) ply 1; (c) ply 2; and (d) ply 3

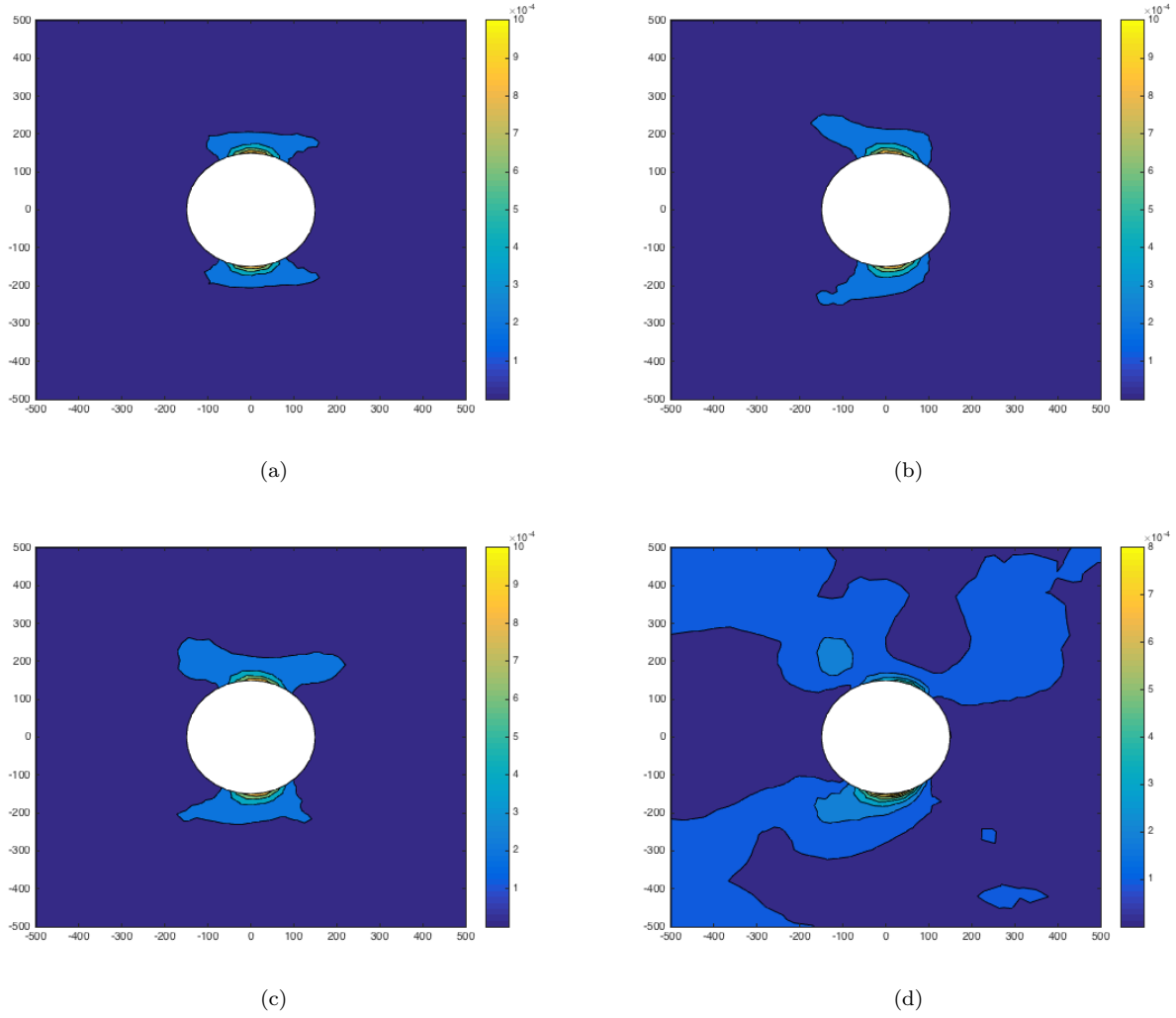

(a) (b)

(c) (d)

Figure 13: Failure index for the design plies: (a) before; and after optimization: (b) ply 1; (c) ply 2; and (d) ply 3

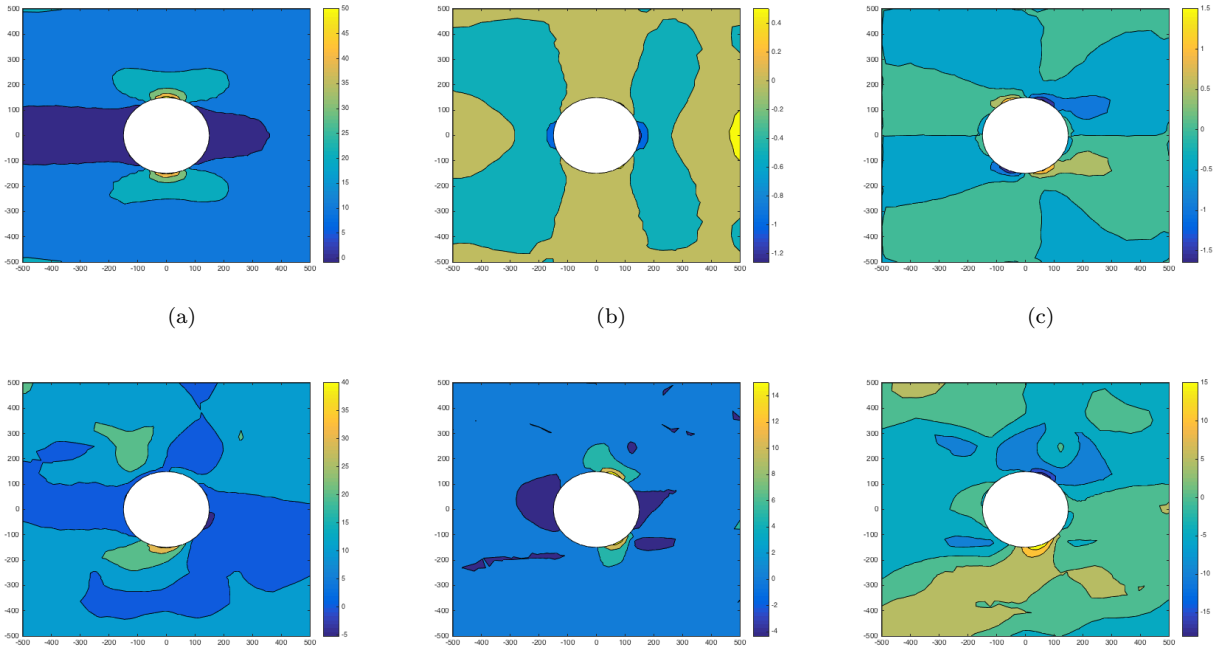

(a) (b) (c)

(d) (e) (f)

Figure 14: Stresses in ply 3 before and after optimization respectively: (a,d) σ_x; (b,e) σ_y; and (c,f) τ_{xy};

V. Conclusion and future work

The proposed framework presented in this manuscript demonstrates the direct use of fiber angles in individual plies as design variables. Multiple test cases (both for static analysis and buckling) were examined to investigate the robustness of the framework. The fiber orientation patterns after optimization corresponds well with optimal patterns known from literature. In addition the proposed framework allows the use of manufacturing constraint, strength constraint, stiffness constraint, etc. during the optimization routine, while the commonly used lamination parameters framework is preferred for pure stiffness based optimization problems only.

Currently a global search optimization approach was used to ensure the global minimum was found, however, this proved to be time consuming. Therefore the future framework will be improved over time to work with different optimizations schemes, in addition to implementing different objective functions and constraint functions.

Another feature is converted the optimized fiber directions into tow paths such that it can be used as input for an automated fiber placement (AFP) machine to manufacture variable stiffness plates. Therefore, a post-processing method was implemented to obtain tow paths from the optimal fiber directions distribution. The workings of the post-processing method is discussed in more detail in previous work of the authors,[17] and therefore not repeated here. A set of optimized fiber directions for a plate with a hole with a coarser mesh than used the previous cases are used as an example to discuss the post-processing method.

As can be seen from Fig. 15, a set of fiber directions (Fig. 15a) was converted to set of feasible tow paths (Fig. 15b). It is important to note that gaps and overlaps are unavoidable when going form a theoretical fiber angle distribution to feasible tow paths inputs for an AFP machine. The gaps and overlaps, however, can be reduced via manual intervention by a manufacturing engineer. In addition, constraint functions in the optimization process can be used to reduce gaps and overlaps or to take the effects of gaps and overlaps on the ABD-matrix into account.

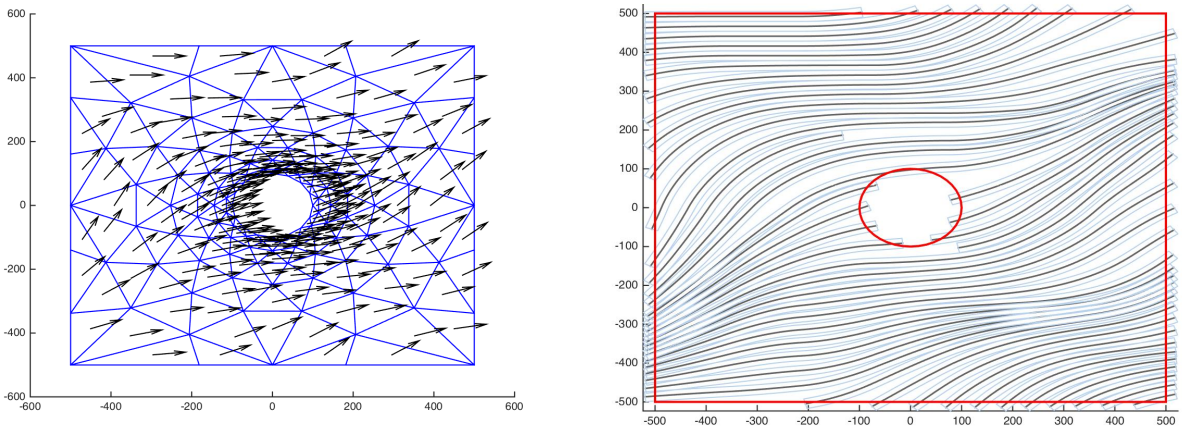

(a) (b)

Figure 15: Post-processing tool result: (a) theoretical fiber angle distribution; and (b) feasible tow paths

References

[1]Li, R., Kelly, D., and Crosky, A., "Strength improvement by fibre steering around a pin loaded hole," *Compos. Struct.*, Vol. 57, No. 1-4, 2002, pp. 377–383.

[2]Gürdal, Z., IJsselmuiden, S., and Campen, J., "Composite Laminate Optimization with Discrete Variables," *Encyclopedia of Aerospace Engineering, R. Blockley, and W. Shyy (eds)*, 2010, pp. 5283–5294.

[3]Gürdal, Z. and Zakhama, R., "Cellular Automata for Simultaneous Analysis and Optimal Structural Topology Design," *Chapter 12 of Simulating Complex Systems by Cellular Automata edited by Kroc, J., Sloot, P.M.A., and Hoekstra, A. Springer*, , No. 1, 2010.

[4]Gürdal, Z., Abdelal, G., and Wu, K., "Experimental and Numerical Evaluation of Thermal Performance of Steered Fibre Composite Laminates," *Chapter 6 of Heat Transfer, Engineering Applications, V.S. Vikhrenko (editor), InTech, Rijeka, Croatia*, 2011, pp. 121–150.

[5]Koon, R., Engelstad, S., Tatting, B., and Gürdal, Z., "Highly Tailored Stiffening for Advanced Composites," 2011.

[6]van Campen, J., Kassapoglou, C., and Gürdal, Z., "Generating Realistic Laminate Fiber Angle Distributions for Optimal Variable Stiffness Laminates," *Composites: Part B, Engineering*, Vol. 43, No. 2, 2012, pp. 354–360.

[7]Khani, A., Abdalla, M., and Gürdal, Z., "Circumferential stiffness tailoring of general cross section cylinders for maximum buckling load with strength constraints," *Comp. Structures*, Vol. 94, No. 9, 2012, pp. 2851–2860.

[8]Tatting, B. and Gürdal, Z., "Design and Manufacture of Elastically Tailored Tow Placed Plates," *NASA/CR2002211919*, 2002.

[9]Tatting, B. and Gürdal, Z., "Automated Finite Element Analysis of Elastically-Tailored Plates," *NASA/CR-2003-212679*, 2003.

[10]Hammer, V., Bendsøe, M., Lipton, R., and Pedersen, P., "Parametrization in laminate design for optimal compliance," *Int. J. Solids Struct.*, Vol. 34, No. 4, 1997, pp. 415–434.

[11]Abdalla, M. M., Setoodeh, S., and Grdal, Z., "Design of variable stiffness composite panels for maximum fundamental frequency using lamination parameters," *Composite Structures*, Vol. 81, No. 2, 2007, pp. 283 – 291.

[12]IJsselmuiden, S., *Optimal Design of Variable Stiffness Composite Structures using Lamination Parameters*, Ph.D. thesis, Delft University of Technology, 2011.

[13]Setoodeh, S., Gürdal, Z., and Watson, L. T., "Design of variable-stiffness composite layers using cellular automata," *Comput. Methods Appl. Mech. Eng.*, Vol. 195, No. 9-12, 2006, pp. 836–851.

[14]Setoodeh, S., Abdalla, M. M., IJsselmuiden, S. T., and Gürdal, Z., "Design of variable-stiffness composite panels for maximum buckling load," *Compos. Struct.*, Vol. 87, No. 1, 2009, pp. 109–117.

[15]Reddy, J., *Mechanics of Laminated Composite Plates and Shells*, CRC Press, Boca Raron (FL), 2nd ed., 2004.

[16]van Tooren, M., Elham, A., Harik, R., and Uddin, A., "Optimal variable stiffness distribution for a composite plate with a row of holes subjected to tension/shear load cases," *16th AIAA/ISSMO Multidisciplinary Analysis and Optimization Conference*, 2015.

[17]van Tooren, M., Jahangir, I., and Elham, A., "Optimization of variable stiffness composite plates with cut-outs subjected to compression, tension and shear using an adjoint formulation," .

[18]van Tooren, M., Harik, R., Elham, A., Lopes, C. S., and Barazanchy, D., "MDO Approach to topimal variable stiffness structure design," *New Trends on Integrity, Reliability and Failure*, 2016.

[19]van Tooren, M., Harik, R., Elham, A., and Barazanchy, D., "Design of variable stiffness composite plates with cut-outs using a dual mesh approach," *Advanced Design Concepts and Practice ADCP 2015 Workshop*, 2015.

[20]MathWorks, "What Is Global Optimization?" `https://www.mathworks.com/help/gads/what-is-global-optimization.html#bsbalkx-1`, 2016, Online; accessed December 10 2016.